

# Elemental Abundances in Two High Column Density Damped Lyman Alpha Systems at $z < 1.5$ <sup>1</sup>

Sandhya M. Rao<sup>2</sup>, Jason X. Prochaska<sup>3,4</sup>, J. Christopher Howk<sup>4,5</sup>, and Arthur M. Wolfe<sup>5</sup>

## ABSTRACT

We present Keck/HIRES abundance measurements and metal-line kinematic profiles of the damped Lyman alpha systems (DLAs) towards the quasars Q0933+733 ( $z_{abs} = 1.479$ ) and Q0948+433 ( $z_{abs} = 1.233$ ). These two DLAs have among the five highest H I column densities at any redshift:  $N(HI) = 4.2 \times 10^{21} \text{ cm}^{-2}$ . The metal-line data, presented here for the first time, reveal that these DLAs are noteworthy for several other reasons as well. 1) The Q0933+733 DLA exhibits simple kinematic structure with unusually narrow velocity widths as measured from its unsaturated metal lines ( $\Delta v = 16 \text{ km s}^{-1}$ ). At 2.6% solar, it has the second lowest metallicity at  $z < 2$ . 2) The Q0948+433 DLA has among the strongest metal-line transitions of any known DLA. The saturated Si II  $\lambda 1808$  line implies a high metallicity ( $[Si/H] > -1$ ) and a significant  $\alpha$ -enhancement. The strong metal lines of this DLA have made possible the detection of Ti II  $\lambda 1910$ , Co II  $\lambda 2012$ , and Mg I  $\lambda 2026$ . 3) We find that the relative gas-phase abundances of both DLAs follow the general trend seen at high redshift, e.g., enhanced Zn/Fe and Si/Fe, and sub-solar Mn/Fe, indicating that there is little evolution in the nucleosynthetic patterns of DLAs down to this epoch. 4) Their high H I column densities imply that these DLAs dominate the column density-weighted cosmic mean metallicity,  $\langle Z \rangle$ , of the universe at  $z < 1.5$ . Using the 15 DLAs with measured metallicities in the redshift interval  $0.4 < z < 1.5$ , we find  $\langle Z \rangle = -0.89_{-0.33}^{+0.40}$ , where the uncertainties are 95% confidence limits.

---

<sup>1</sup>Based on data obtained with the NASA/ESA *Hubble Space Telescope* operated by STScI-AURA under NASA contract NAS 5-26555.

<sup>2</sup>Department of Physics & Astronomy, University of Pittsburgh, Pittsburgh, PA 15260; rao@everest.phyast.pitt.edu

<sup>3</sup>UCO/Lick Observatory, University of California, Santa Cruz, CA 95064

<sup>4</sup>Department of Physics, and Center for Astrophysics and Space Sciences, University of California, San Diego, C-0424, La Jolla, CA 92093

<sup>5</sup>Visiting Astronomer, W. M. Keck Telescope. The Keck Observatory is a joint facility of the University of California and the California Institute of Technology.

*Subject headings:* galaxies: abundances — quasars: absorption lines — quasars: individual (Q0933+733, Q0948+433)

## 1. Introduction

It has been known for almost two decades now that damped Lyman alpha systems (DLAs) seen in the spectra of background quasars trace the neutral gas content of the universe back to the redshifts of the most distant quasars (Wolfe et al. 1986). This fact has since been exploited to study the evolution of the neutral gas content of the universe (e.g., Lanzetta et al. 1991, Peroux et al. 2003, Rao & Turnshek 2000 [RT00], Storrie-Lombardi & Wolfe 2000; Prochaska & Herbert-Fort 2004) and its chemical enrichment history (e.g., Pettini et al. 1999, Prochaska et al. 2003b, and references therein). Until recently, however, the rarity of DLAs in combination with the requirement of the *Hubble Space Telescope* to discover them at redshifts  $z < 1.65$  has meant that most of our knowledge about the galaxies that contain the bulk of the neutral gas has come from objects that span only the first 30% of the age of the universe.

High resolution spectrometers on 10m-class telescopes have been instrumental in advancing our knowledge about the detailed abundance patterns and kinematic properties of DLAs (e.g. Pettini et al. 1999; Pettini et al. 2000; Molaro et al. 2000; Prochaska et al. 2001; Ledoux, Bergeron, & Petitjean 2002; Prochaska & Wolfe 2002; Dessauges-Zavadsky et al. 2004). This work has mainly concentrated on the large sample of  $z > 1.65$  DLAs known to date. With the success of UV surveys for DLAs at redshifts  $z < 1.65$  (RT00; Rao, Turnshek, & Nestor 2004), the number of DLAs available for study at these redshifts has been steadily increasing and it is now becoming possible to fill in the large gap in cosmic time between today and  $z \sim 2$ . The importance of studying low-redshift DLAs cannot be understated: these systems bridge the gap between our knowledge of present-day galaxies and high-redshift DLAs. The low-redshift systems are the only population (currently) of cosmological objects for which the neutral gas content, abundances, and kinematic properties obtained via high resolution spectroscopy can be compared with observable galaxy properties such as morphology and star formation history.

To date, only a handful of  $z < 1.5$  DLAs have been observed with high resolution spectroscopy (e.g. Pettini et al. 1999, 2000). These observations showed that the abundance ratios and general kinematic properties of lower-redshift DLAs are similar to those at higher redshift. Here we add to the growing list of DLA abundance measurements at  $z < 1.65$  with Keck/HIRES data on the DLAs towards the quasars Q0933+733 ( $z_{abs} = 1.479$ ) and Q0948+433 ( $z_{abs} = 1.233$ ). With  $N(HI) = 4.2 \times 10^{21} \text{ cm}^{-2}$  (§2.1), these two DLAs rank

among the five highest H I column density systems known. High column density DLAs are important for follow-up metallicity observations for two reasons. First, their high column density may allow the measurement of weak lines rarely observed in DLAs. For example, we report a  $> 3\sigma$  detection of Co II  $\lambda 2012$  in the Q0948+433,  $z = 1.233$ , DLA (§3.2). This is the second detection of Co to date (Ellison, Ryan, & Prochaska 2001) and the most secure. Its detection promises the observation of weak transitions of even rarer elements (e.g., Cu, Ga, B, etc.). Second, the highest column density DLAs dominate the determination of cosmic metallicity since cosmic metallicity is given by an H I column density-weighted mean. Thus, the current measurement of the cosmological mean metallicity in neutral gas at  $z \approx 1.4$  is dominated by these two DLAs. This paper is organized as follows. In §2 we describe the observations and data reduction techniques. The metal-line profiles and chemical abundances of the two DLAs are presented in §3. We conclude with a discussion in §4.

## 2. Observations

### 2.1. *HST* data

#### 2.1.1. *Q0933+733*

*HST*-UV spectroscopic data for Q0933+733 were obtained as part of a Cycle 6 survey for DLAs in known  $z < 1.65$  Mg II absorption-line systems (*HST* PID 6577, S. Rao PI; RT00). This  $z_{em} = 2.525$  quasar has two strong Mg II systems along the sightline at  $z = 1.4789$  and  $z = 1.4973$  (Steidel & Sargent 1992). Figure 10 of RT00 shows the *HST*-FOS G270H grating spectrum of Q0933+733. Since the Ly $\alpha$  profiles of the two absorbers are blended with each other and with a Lyman limit edge, the H I column density of the DLA at  $z = 1.479$  was determined using the Ly $\beta$  absorption line (see figure 11 of RT00), and was found to be  $(4.2 \pm 0.8) \times 10^{21} \text{ cm}^{-2}$ . The higher redshift system, which also has detectable Ly $\beta$  absorption, has an HI column density  $N(HI) = (1.0 \pm 0.5) \times 10^{20} \text{ cm}^{-2}$  (Rao et al. 2004) just below the DLA criterion, and we reserve an analysis of this absorber to a future paper. The uncertainty in these two column density measurements reflects the low signal-to-noise ratio of the spectrum near the Ly $\beta$  lines.

#### 2.1.2. *Q0948+433*

This quasar was observed with *HST*-STIS as part of another DLA survey for strong Mg II absorption-line systems found in optical spectra of quasars (*HST* PID 9051, R. Becker

PI). The data, which we obtained from the *HST* public archive, consist of two exposures taken with the G230L grating for a total of 2,333 seconds. We combined the two sub-exposures using a weighted average based on exposure time and combined the error arrays accordingly. We then normalized the resulting spectrum using standard routines in IRAF. Since there are Lyman limit edges in this spectrum, only a local continuum near the DLA line was determined. Part of the normalized *HST* archive spectrum encompassing the DLA line is shown in Figure 1. As is usually the case for high column density DLA lines, the Ly $\alpha$  forest populates the DLA trough making it very difficult to use a routine such as least squares minimization to fit a Voigt profile to the data. Therefore, the best ‘fit’ was estimated by eye. A Voigt profile with column density  $N(HI) = 4.2 \times 10^{21} \text{ cm}^{-2}$  convolved with the Gaussian line spread function of the *HST*-STIS G230L grating is shown as the dotted line in Figure 1. The uncertainty in the column density determination,  $0.5 \times 10^{21} \text{ cm}^{-2}$  in this case, is dominated by the error in continuum placement and was estimated using the procedure described in RT00.

## 2.2. Keck/HIRES data

Q0933+733 and Q0948+433 were observed with Keck/HIRES (Vogt et al. 1994) on UT 2003 March 11 and 12 for a total integration time of 5,400s each. For both sets of observations, we implemented the C1 decker (0.86" width; FWHM  $\approx 6 \text{ km s}^{-1}$  resolution) and the kv380 filter to block second order light. Data reduction and calibration proceeded in standard fashion (e.g. Prochaska et al. 2001) with the MAKEE reduction package kindly provided by T. Barlow. The data were continuum fit with custom software and rebinned to  $2 \text{ km s}^{-1}$  per pixel. The signal-to-noise ratio of these data exceeds 20 per pixel for the majority of the Q0933+733 spectrum and is greater than 10 per pixel redward of  $4500\text{\AA}$  in the Q0948+433 spectrum.

## 3. Metal-Line Profiles and Chemical Abundances

All of the ionic column densities were derived with the apparent optical depth method (AODM; Savage & Sembach 1991; Jenkins 1996). This technique can be used to identify hidden saturation by comparing the apparent column densities of multiple transitions from a single ion. This technique also gives an efficient, non-parametric means of calculating total column densities for each ion. For those transitions where the profile saturates in at least one pixel (i.e., normalized flux  $< 0.05$ ), the column densities are listed as lower limits. We report non-detections as  $3\sigma$  statistical upper limits. We have ignored continuum error in

our analysis which may dominate the measurements of very weak transitions. We estimate a systematic error  $< 10\%$  in most cases due to continuum placement. We calculate ionic column densities for each transition and assign final column densities by calculating the weighted-mean for ions with multiple transitions. In the velocity plots,  $v = 0$  is chosen arbitrarily and corresponds to the redshift listed in the figure caption. We indicate regions of blending, primarily through blends with other metal-line systems or the Ly $\alpha$  forest, by plotting with dotted lines.

The atomic data considered in this paper are listed in Table 1. Table 2 gives our assumed solar abundance data compiled by Grevesse & Sauval (1999).

### 3.1. Q0933+733; $z=1.479$

The metal line profiles of this  $z = 1.479$  DLA are shown in Figure 2. The profiles are remarkably narrow with a velocity width  $\Delta v = 16 \text{ km s}^{-1}$ , where  $\Delta v$  is the interval encompassing 90% of the total optical depth (Prochaska & Wolfe 1997), and is measured using the unsaturated Zn II 2026 profile. This is among the lowest  $\Delta v$  value recorded for a DLA (Prochaska & Wolfe 2001). We also note a likely ‘edge-leading asymmetry’ for the profiles towards positive velocities in the unsaturated metal lines, consistent with rotation. This characterization, however, is limited by the fact that the profile is only  $\approx 2$  resolution elements wide.

We have integrated the line profiles using the AODM to calculate the ionic column densities given in Table 3. Columns 1 and 2 list the ion and rest wavelength, column 3 gives the column density, column 4 is the weighted mean column density determined from multiple absorption lines of the same ion, and is listed alongside the first occurrence of the ion, and column 5 is the derived abundance relative to solar. Comparisons of multiple transitions from a given ion (e.g. Cr II) are in reasonable agreement and there is no indication of line saturation. We note, however, that the Cr II  $\lambda 2062$  and Zn II  $\lambda 2062$  column densities are lower than their partner transitions which may indicate that the continuum level is systematically low in this region.

Measurements of Zn and Si indicate a metallicity  $\sim 1/40$  solar which falls  $\approx 0.5$  dex below the mean metallicity at  $z \sim 2$ . The value lies at the lower end of the DLA metallicity distribution at these redshifts and is the second lowest value recorded at  $z < 2$ . Figure 3 describes the relative abundances for this DLA system. As is standard practice in stellar abundance studies, and now generally adopted to describe DLA abundances, we plot measured abundances relative to Fe (top panel). This comparison serves to illustrate the

combined effects of dust depletion and nucleosynthesis (e.g. Prochaska & Wolfe 2002). The bottom panel gives the absolute abundances on a logarithmic scale where hydrogen has value 12.0. In both cases we present gas-phase abundances, i.e., the observed values uncorrected for depletion.

Similar to the results for other  $z \sim 1.5$  DLAs (Pettini et al. 1999) and the majority of  $z > 2$  DLAs (Prochaska & Wolfe 2002), this DLA shows modest enhancements of Zn and Si relative to Fe. These enhancements are suggestive of differential depletion and/or nucleosynthetic processes, and it is difficult to disentangle the two effects. The Cr/Fe overabundance relative to solar is notable as it exceeds the value observed for Cr/Fe in the majority of Milky Way sightlines (e.g. Savage and Sembach 1996). Prochaska & Wolfe (2002) reported a similar enhancement for their sample of high  $z$  DLAs and suggested that it is a signature of nucleosynthesis. Interestingly, the enhancement runs contrary to the behavior of Cr in metal-poor halo stars where [Cr/Fe] decreases with [Fe/H] (McWilliam et al. 1995). Although this is only a modest departure from the solar ratio, it suggests differences in the yields of Fe-peak elements.

Finally, we note sub-solar Ti/Fe and Mn/Fe ratios. As emphasized by Dessauges-Zavadsky, Prochaska, & D’Odorico (2002), Mn and Ti are particularly valuable for disentangling the competing effects of nucleosynthesis and differential depletion. The sub-solar Ti/Fe ratio observed here is indicative of differential depletion, and is somewhat surprising given the low dust depletion levels implied by the relatively low Zn/Fe ratio. Perhaps the low Ti/Fe ratio is more reflective of grain core growth as opposed to grain mantle growth and, in turn, an important clue to the mechanism of grain formation in young, metal-poor galaxies (e.g., supernovae, red giant winds). In contrast to Ti, the observed low Mn/Fe ratio is a reflection of nucleosynthesis. The sub-solar value follows previous measurements of Mn/Fe (Pettini et al. 2000; Ledoux, Bergeron, & Petitjean 2002) and supports the notion that Mn production is metallicity-dependent (McWilliam, Rich, & Smecker-Hane 2003).

We note that except for Ti II and Fe II, the results of Khare et al. (2004) agree with our measurements for this DLA. Their Multiple Mirror Telescope (*MMT*) spectra do not have the high resolution and signal-to-noise ratio per pixel that characterize our Keck data. Thus, we believe that the Ti II column density is indeed an upper limit as shown in Table 3, rather than a confirmed detection as claimed by Khare et al. (2004). In addition, our Fe abundance is more secure since Khare et al. (2004) used the equivalent widths of lines measured by Steidel & Sargent (1992) and an assumed  $b$  parameter to estimate its column density.

### 3.2. Q0948+433; z=1.233

The metal line profiles of the damped Ly $\alpha$  system at  $z = 1.233$  are shown in Figure 4. The line profiles show greater complexity than the DLA toward Q0933+733 although the observed velocity width ( $\Delta v = 68 \text{ km s}^{-1}$ ) is still lower than the median value at  $z > 2$ . We also note that the line profiles show the ‘edge-leading’ characteristic of many high  $z$  DLAs (Prochaska & Wolfe 1997) and a mild asymmetry to the line profiles. Again, these characteristics are consistent with rotation.

The metal-line transitions of this DLA are among the strongest ever observed. Note, in particular, the saturated Si II  $\lambda 1808$  profile which implies  $N(\text{SiII}) > 10^{16} \text{ cm}^{-2}$  and  $[\text{Si}/\text{H}] > -1$  dex. This Si II  $\lambda 1808$  profile is deeper than that observed for almost any sightline through the Milky Way<sup>1</sup>. We find, therefore, that this ‘metal-strong’ DLA shows positive detections of weak transitions like Ti II  $\lambda 1910$ , Co II  $\lambda 2012$ , and Mg I  $\lambda 2026$ . We note that for the Ti II  $\lambda 1910$  doublet, we integrated the optical depth over both transitions and used the sum of the oscillator strengths to convert that optical depth to column density. The column densities for all of the detected transitions are listed in Table 4. We predict that the Cr II 2026 transition contributes  $< 5\%$  to the Zn II 2026 profile and have ignored this blend in our analysis.

The relative abundances of this DLA are presented in Figure 5. The abundance pattern of Cr, Mn, Zn, and Fe is similar to that of the DLA system toward Q0933+733: Cr/Fe and Zn/Fe show modest enhancements and Mn/Fe is significantly underabundant. In addition, we report the second detection of Co to date. In contrast to the first detection of Co by Ellison et al. (2001) in the Q2206–199 DLA system<sup>2</sup>, which is overabundant relative to Fe, we find a solar Co/Fe abundance ratio in the Q0948+433 DLA. Ellison et al. show that the overabundance in the Q2206–199 DLA is consistent with the pattern seen in Galactic bulge stars. The solar Co/Fe ratio and observed metallicity (e.g.,  $[\text{Fe}/\text{H}]$ ) in the Q0948+433 DLA, on the other hand, are more typical of metal-rich Galactic halo stars (Gratton & Sneden 1991). While it is impossible to establish trends with only two systems, it is at least evident that their  $[\text{Co}/\text{Fe}]$  ratios fall within the locus traced by Galactic stars.

Perhaps the most interesting result of these observations is that both Si and Ti<sup>3</sup> (the  $\alpha$ -elements) are significantly enhanced relative to Fe. Since Ti is more readily adsorbed onto

---

<sup>1</sup>Due to depletion of Si from the gas-phase in Milky Way sightlines with large  $N(\text{HI})$  and because sight lines observed in the Milky Way at high resolution tend to have lower  $N(\text{HI})$ .

<sup>2</sup>But see Prochaska & Wolfe (2002) who do not consider this detection to be very secure.

<sup>3</sup>One may view the Ti result cautiously because of the relatively poor S/N at the Ti II 1910 transitions.

dust grains than Fe (e.g. Savage and Sembach 1996), differential depletion leads to negative values for [Ti/Fe]. Therefore, the observed enhancement (i.e., positive [Ti/Fe]) is not due to depletion, but implies a nucleosynthetic origin instead. This characteristic is, as in the case of the Co/Fe ratio discussed above, typical of Galactic halo stars (e.g., Gratton & Sneden 1991). If one were to correct for differential depletion in this DLA, by using the Cr/Zn ratio for example, the dust-corrected Ti/Fe ratio may exceed +0.4 dex. Differential depletion could be invoked to explain the large Si/Fe ratio, but we emphasize that [Si/Zn] > +0.1, and given the significant line saturation in Si II $\lambda$ 1808, the Si/Zn ratio may exceed +0.3 dex. Altogether, these relative abundances indicate a significant  $\alpha$ -enhancement in this modest metallicity gas. This result contradicts a primary conclusion of Pettini et al. (2000) who argued that the low  $z$  DLA systems have solar  $\alpha$ /Fe ratios and therefore may not trace the bulk of star formation. We note that the abundance pattern and metallicity mirror those observed for the most metal-rich Galactic halo stars (e.g. Edvardsson et al. 1993) and the Galactic thick disk stars (Prochaska et al. 2000). Perhaps we are observing the by-products of the generation of star formation which immediately proceeds the formation of the galactic disk in this system, a speculation supported by the ‘edge-leading’ nature of the metal-line profiles.

#### 4. Discussion

The DLAs towards Q0933+733 and Q0948+433 are unusual in several ways. At  $4.2 \times 10^{21} \text{ cm}^{-2}$ , their H I column densities are among the five highest at any redshift of over 150 DLAs with measured metallicities, and so they dominate the column density-weighted mean metallicity of the universe at  $z \approx 1.4$ . Here we update the Prochaska et al. (2003b) estimate of the column-density weighted mean metallicity for the redshift interval  $0.4 < z < 1.5$ . We add the Q0933+733 DLA to the sample, and use a revised value for the H I column density of the Q0948+433 DLA. We also include the recent results of Turnshek et al. (2004) and Khare et al. (2004). Table 5 lists the data used to determine the column density-weighted mean metallicity,  $\langle Z \rangle = \log[\sum_i 10^{[M/H]_i} N(HI)_i / \sum_i N(HI)_i]$ . We find  $\langle Z \rangle = -0.89_{-0.33}^{+0.40}$  at a median redshift of  $\langle z \rangle = 0.86$ , where the uncertainties have been estimated using the bootstrap technique and are 95% confidence limits. This result is shown in Figure 6 along with high-redshift measurements from Prochaska et al. (2003b). The new low-redshift value of  $\langle Z \rangle$  is in agreement with the value estimated by Prochaska et al. (2003b), but with significantly smaller uncertainty. We also confirm the trend of increasing metallicity with cosmic time and, from a least-squares fit to the  $\langle Z \rangle$  values, derive a slope of  $m = -0.26 \pm 0.06$ .

The narrow velocity width of the Q0933+733 DLA,  $\Delta v = 16 \text{ km s}^{-1}$ , implies a kine-



matically simple system, while the edge-leading asymmetries of the unsaturated lines reveal structure even on these small velocity scales. Although the metal line profiles of the Q0948+433 DLA have several components, their combined velocity width of  $\Delta v = 68 \text{ km s}^{-1}$  is still lower than the median value measured for DLAs. Both DLAs follow the trend first noted by Wolfe & Prochaska (1998), which is still evident in the larger sample of Prochaska et al. (2003a), that high  $N(HI)$  DLAs tend to have smaller metal-line velocity widths. The compilation of 21 cm line widths by Kanekar & Chengalur (2003) indicates that a similar trend might be present between 21 cm line widths and  $N(HI)$ . Additionally, Nestor et al. (2003) found a correlation between DLA metallicity and Mg II rest equivalent width, the latter being an indicator of the velocity spread along the line of sight. Thus, a comprehensive study of 21 cm absorption line properties, H I column densities, metallicities, and metal line profiles for DLAs in front of radio loud quasars might provide some insight into the nature of the individual cloud(s) that gives rise to a DLA system.

The high  $N(HI)$  value of the Q0933+733 DLA ensures that many metal-line transitions are easily measured even at a metallicity as low as 2.6% solar (§3.1). This is the second lowest value recorded at  $z < 2$ . Even so, relative abundance patterns in this DLA are similar to results for other DLAs, implying that there is minimal evolution in the nucleosynthetic patterns for gas with  $[M/H] < -1$  at this epoch.

Finally, the Q0948+433 DLA is characterized by the highly saturated Si II  $\lambda 1808$  line, which implies a high metallicity ( $[Si/H] > -1$ ) and a significant  $\alpha$ -enhancement. The unusually strong lines of this DLA have made possible the detections of Ti II  $\lambda 1910$ , Co II  $\lambda 2012$ , and Mg I  $\lambda 2026$ , and we further predict that echelle observations to the atmospheric limit would reveal positive detections of transitions for Ga, P, Ge, Sn, and possibly Pb. Since the mean metallicity of the DLAs is observed to increase with decreasing redshift, a large sample of  $z < 1.5$  DLAs may be more likely to yield ‘metal-strong’ candidates. Therefore, surveys of these galaxies may be the most efficient approach to obtain comprehensive abundance pattern measurements of young galaxies, and given the recent loss of STIS on HST, emphasizes the need for a UV spectrograph in space.

S.R. gratefully acknowledges Dave Turnshek for many helpful discussions. The space-based component of this work has been funded in part by NASA-LTSA grant NAG5-7930. The authors wish to recognize and acknowledge the very significant cultural role and reverence that the summit of Mauna Kea has always had within the indigenous Hawaiian community. We are most fortunate to have the opportunity to conduct observations from this mountain. We acknowledge the Keck support staff for their efforts in performing these observations. J.X.P. and A.M.W. are partially supported by NSF grant AST0307824.

## REFERENCES

- S.D. & Lawler, J.E. 1993, ApJ, 408, 382
- Bergeson, S.D. & Lawler, J.E. 1993b, ApJ, 414, L137
- Bergeson, S.D., Mullman, K.L., & Lawler, J.E. 1993, ApJ, 435, L157
- Boissé, P., Le Brun, V., Bergeron, J., & Deharveng, J.-M. 1998, A&A, 333, 841
- Churchill, C. W., Mellon, R. R., & Charlton, J. C. et al. 2000, ApJS, 130, 91
- de la Varga, A., Reimers, D., Tytler, D., Barlow, T. A., & Burles, S. 2000, A&A, 363, 69
- J.X., & D’Odorico, S. 2002, A&A, 391, 801
- Dessauges-Zavadsky, M., Calura, F., Prochaska, J.X., D’Odorico, S., & Matteucci, F. 2004, A&A, 416, 79
- paper Edvardsson, B., Anderson, J., Gutasfsson, B., Lambert, D.L., Nissen, P.E., and Tompkin, J. 1993, A&A, 275, 101
- Ellison, S.L., Ryan, S., & Prochaska, J.X. 2001, MNRAS, 326, 628
- J. A., Wiese, L. M., & Lawler, J. E. 2000, ApJ, 538, 773
- abundances Gratton, R.G. & Sneden, C. 1991, A&A, 241, 501
- Grevesse, N. & Sauval, A.J. 1999, A&A, 347, 348
- Jenkins, E. B. 1996, ApJ, 471, 292
- Kanekar, N., & Chengalur, J. N. 2003, A&A, 399, 857
- Khare, P., Kulkarni, V. P., Lauroesch, J. T., York, D. G., Crofts, A. P. S., & Nakamura, O. 2004, astro-ph/0408139
- Lanzetta, K. M., Wolfe, A. M., Turnshek, D. A., Lu, L., McMahon, R. G., & Hazard, C. 1991, ApJS, 71, 1
- Ledoux, C., Bergeron, J., & Petitjean, P. 2002, A&A, 385, 802
- Paper II McWilliam, A., Preston, G.W., Sneden, C., & Searle, L. 1995, AJ, 109, 2757
- McWilliam, A., Rich, R.M., & Smecker-Hane, T.A. 2003, ApJ, 592, L21

- Meyer, D. M., Lanzetta, K. M., & Wolfe, A. M. 1995, *ApJ*, 451, L13
- Molaro, P., Bonifacio, P., Centurión, M., D’Odorico, S., Vladilo, G., Santin, P., & Di Marcantonio, P. 2000, *ApJ*, 541, 54
- Morton, D.C. 1991, *ApJS*, 77, 119
- Morton, D.C. 2004, priv. comm.
- K. L., Lawler, J. E., Zsargo, J., & Federman, S. R. 1998, *ApJ*, 500, 1064
- Nestor, D. B., Rao, S., Turnshek, D. A., & Vanden Berk, D. 2003, *ApJ*, 595, L5
- Péroux, C., McMahon, R. G., Storrie-Lombardi, L. J., & Irwin, M. J. 2003, *MNRAS*, 346, 1103
- Pettini, M., Ellison, S. L., Steidel, C. C., & Bowen, D. V. 1999, *ApJ*, 510, 576
- Pettini, M., Ellison, S. L., Steidel, C. C., Shapley, A. E., & Bowen, D. V. 2000, *ApJ*, 532, 65
- Pettini, M., Ellison, S. L., Bergeron, J., & Petitjean, P. 2002, *A&A*, 391, 21
- J. X., Naumov, S.O., Carney, B.W., McWilliam, A., & Wolfe, A.M. 2000, *AJ*, 120, 2513
- Prochaska, J.X., Wolfe, A.M., Tytler, D., Burles, S.M., Cooke, J., Gawiser, E., Kirkman, D., O’Meara, J.M., & Storrie-Lombardi, L. 2001, *ApJS*, 137, 21
- Prochaska, J. X. & Wolfe, A. M. 1997, *ApJ*, 487, 73
- Prochaska, J. X. & Wolfe, A. M. 1998, *ApJ*, 507, 113
- Prochaska, J.X. & Wolfe, A.M. 2001, *ApJ*, 560, L33
- Prochaska, J.X. & Wolfe, A.M. 2002, *ApJ*, 566, 68
- Prochaska, J.X. & Herbert-Fort, S. 2004, *PASP*, in press
- Prochaska, J.X., Gawiser, E., Wolfe, A.M., Cooke, J., & Gelino, D. 2003a, *ApJS*, 147, 227
- Prochaska, J.X., Gawiser, E., Wolfe, A.M., Castro, S., & Djorgovski, S.G. 2003b, *ApJ*, 595, L9
- Rao, S., & Turnshek, D. 2000, *ApJS*, 130, 1 (RT00)
- Rao, S., Turnshek, D., & Nestor, D. 2004, in preparation

- Savage, B. D. and Sembach, K. R. 1991, *ApJ*, 379, 245
- Savage, B. D. and Sembach, K. R. 1996, *ARA&A*, 34, 279
- Steidel, C. C., & Sargent, W. L. W. 1992, *ApJS*, 80, 1
- Storrie-Lombardi, L., & Wolfe, A. M. 2000, *ApJ*, 543, 552
- Turnshek, D. A., Rao, S. M., Ptak, A. F., Griffiths, R. E., & Monier, E. M. 2003, *ApJ*, 590, 730
- Turnshek, D. A., Rao, S. M., Nestor, D. B., Vanden Berk, D., Belfort-Mihaly, M., & Monier, E. M. 2004, *ApJ*, 609, L53
- Verner, D. A., Barthel, P. D., Tytler, D. 1994, *A&AS*, 108, 287
- Vladilo, G. 2002, *A&A*, 391, 407
- Vogt, S.S., Allen, S.L., Bigelow, B.C., Bresee, L., Brown, B., et al. 1994, *SPIE*, 2198, 362
- Wiese, L.M., Fedchak, J. A., & Lawler, J. E. 2001, *ApJ*, 547, 1178
- Wolfe, A. M., Turnshek, D. A., Smith, H. E., & Cohen, R. D. 1986, *ApJS*, 61, 249
- Wolfe, A.M. & Prochaska, J.X. 1998, *ApJ*, 494, 15L

Table 1. ATOMIC DATA

Transition	$\lambda$	$f$	Ref
Cl 1656	1656.9283	0.1405	1
AlII 1670	1670.7874	1.8800	1
PbII 1682	1682.150	0.15636	1
NiII 1741	1741.5531	0.0427	7
NiII 1751	1751.9157	0.0277	7
SiII 1808	1808.0130	0.00218600	11
AlIII 1854	1854.7164	0.539	1
AlIII 1862	1862.7895	0.268	1
TiII 1910a	1910.6000	0.202	12
TiII 1910b	1910.9380	0.098	12
CoII 2012	2012.1664	0.03679	8
ZnII 2026	2026.1360	0.489	13
CrII 2026	2026.269	0.00471	15
MgI 2026	2026.4768	0.1120	1
CrII 2056	2056.2539	0.105	13
CrII 2062	2062.2340	0.078	13
ZnII 2062	2062.6640	0.256	13
CrII 2066	2066.1610	0.0515	13
FeII 2249	2249.8768	0.00182100	14
FeII 2260	2260.7805	0.00244	14
FeII 2344	2344.2140	0.114	3
FeII 2374	2374.4612	0.0313	3
FeII 2382	2382.7650	0.320	3
MnII 2576	2576.8770	0.3508	1
FeII 2586	2586.6500	0.0691	3
MnII 2594	2594.4990	0.271	1
FeII 2600	2600.1729	0.239	3
MnII 2606	2606.462	0.1927	1
MgII 2796	2796.3520	0.6123	15
MgII 2803	2803.5310	0.3054	15
MgI 2852	2852.9642	1.810	1

References. — 1: Morton (1991); 3: Morton (2004); 7: Fedchak, Wiese, & Lawler (2000); 8: Mullman et al. (1998); 11: Bergeson & Lawler (1993b); 12: Wiese, Fedchak, &

Lawler (2001); 13: Bergeson & Lawler (1993);  
14: Bergeson, Mullman, & Lawler (1994); 15:  
Verner et al. (1994)

Table 2. ADOPTED SOLAR ABUNDANCES

Elm	$\epsilon(X)$	Z
H	12.00	1
B	2.79	5
Mg	7.58	12
Al	6.49	13
Si	7.56	14
S	7.20	16
Ti	4.94	22
Cr	5.67	24
Mn	5.53	25
Fe	7.50	26
Co	4.91	27
Ni	6.25	28
Zn	4.67	30

Table 3. IONIC COLUMN DENSITIES: Q0933+733,  $z = 1.479$

Ion	$\lambda$	AODM <sup>a</sup>	$N_{\text{adopt}}$	[X/H]
H I	1215.7		$21.62^{+0.10}_{-0.10}$	
C I	1656.9	< 12.737		
Al II	1670.8	> 13.367	> 13.367	> -2.743
Al III	1854.7	$12.718 \pm 0.036$		
Al III	1862.8	$12.472 \pm 0.094$		
Si II	1808.0	> 15.555	> 15.555	> -1.625
Ti II	1910.6	< 12.433	< 12.433	< -2.127
Cr II	2056.3	$13.584 \pm 0.016$	$13.563 \pm 0.012$	$-1.727 \pm 0.101$
Cr II	2062.2	$13.510 \pm 0.023$		
Cr II	2066.2	$13.606 \pm 0.029$		
Mn II	2576.9	$12.962 \pm 0.013$	$12.957 \pm 0.011$	$-2.193 \pm 0.101$
Mn II	2606.5	$12.947 \pm 0.018$		
Fe II	2249.9	$15.178 \pm 0.016$	$15.190 \pm 0.011$	$-1.930 \pm 0.101$
Fe II	2260.8	$15.203 \pm 0.016$		
Fe II	2344.2	> 14.511		
Fe II	2374.5	> 14.882		
Fe II	2382.8	> 14.110		
Fe II	2586.7	> 14.649		
Fe II	2600.2	> 14.185		
Co II	2012.2	< 12.969	< 12.969	< -1.561
Ni II	1741.6	$13.916 \pm 0.014$	$13.922 \pm 0.011$	$-1.948 \pm 0.101$
Ni II	1751.9	$13.936 \pm 0.020$		
Zn II	2026.1	$12.748 \pm 0.019$	$12.712 \pm 0.019$	$-1.578 \pm 0.102$
Zn II	2062.7	$12.551 \pm 0.058$		
Pb II	1682.2	< 12.320	< 12.320	< 0.640

<sup>a</sup>Errors reflect statistical uncertainty. One should adopt an additional 15% systematic error for weak transitions due to continuum uncertainty.



Table 4. IONIC COLUMN DENSITIES: Q0948+433,  $z = 1.233$

Ion	$\lambda$	AODM <sup>a</sup>	$N_{\text{adopt}}$	[X/H]
H I	1215.7		$21.62^{+0.05}_{-0.06}$	
Mg I	2026.5	$13.069 \pm 0.044$		
Mg I	2853.0	$> 12.878$		
Mg II	2796.4	$> 14.036$	$> 14.306$	$> -2.894$
Mg II	2803.5	$> 14.306$		
Al III	1854.7	$13.111 \pm 0.045$		
Al III	1862.8	$13.119 \pm 0.088$		
Si II	1808.0	$> 16.147$	$> 16.147$	$> -1.033$
Ti II	1910.6	$13.339 \pm 0.070$	$13.339 \pm 0.070$	$-1.221 \pm 0.092$
Cr II	2056.3	$13.912 \pm 0.016$	$13.905 \pm 0.014$	$-1.385 \pm 0.062$
Cr II	2066.2	$13.889 \pm 0.025$		
Mn II	2576.9	$13.368 \pm 0.015$	$13.305 \pm 0.012$	$-1.845 \pm 0.061$
Mn II	2594.5	$13.249 \pm 0.025$		
Mn II	2606.5	$13.253 \pm 0.024$		
Fe II	2249.9	$15.536 \pm 0.019$	$15.563 \pm 0.013$	$-1.557 \pm 0.061$
Fe II	2260.8	$15.595 \pm 0.018$		
Fe II	2344.2	$> 14.676$		
Fe II	2374.5	$> 15.209$		
Fe II	2382.8	$> 14.296$		
Fe II	2586.7	$> 14.870$		
Co II	2012.2	$13.025 \pm 0.119$	$13.025 \pm 0.119$	$-1.505 \pm 0.133$
Zn II	2026.1	$13.152 \pm 0.013$	$13.152 \pm 0.013$	$-1.138 \pm 0.061$

<sup>a</sup>Errors reflect statistical uncertainty. One should adopt an additional 15% systematic error for weak transitions due to continuum uncertainty.

Table 5.  $0.4 < z < 1.5$  Sample of DLA Metallicities

QSO	$z_{abs}$	$\log N(HI)$	[M/H]	$f_{[M/H]}^a$	Refs.
Q1229–021	0.395	$20.75 \pm 0.07$	$-0.47 \pm 0.15$	1	a
Q0235+164	0.526	$21.65 \pm 0.04$	$-0.58 \pm 0.15$	2	b
Q1622+238	0.656	$20.36 \pm 0.10$	$-0.87 \pm 0.25$	3	c, d
Q1122–168	0.682	$20.45 \pm 0.05$	$-1.00 \pm 0.15$	3	e
Q1328+307	0.692	$21.25 \pm 0.06$	$-1.20 \pm 0.09$	1	f
Q1323-0021	0.716	$20.54 \pm 0.15$	$0.04 \pm 0.16$	1	g,h
Q1107+0048	0.740	$21.00 \pm 0.05$	$-0.64 \pm 0.07$	1	g,h
Q0454+039	0.860	$20.69 \pm 0.06$	$-0.79 \pm 0.12$	4	i
Q1727+5302	0.945	$21.16 \pm 0.04$	$-0.58 \pm 0.15$	1	j
...	1.031	$21.41 \pm 0.04$	$-1.32 \pm 0.38$	1	j
Q0302–223	1.009	$20.36 \pm 0.11$	$-0.73 \pm 0.12$	4	i
Q0948+433	1.233	$21.62 \pm 0.05$	$-1.14 \pm 0.06$	1	k
Q0935+417	1.373	$20.52 \pm 0.10$	$-0.94 \pm 0.13$	1	f
Q1354+258	1.420	$21.54 \pm 0.06$	$-1.61 \pm 0.16$	1	i
Q0933+733	1.479	$21.62 \pm 0.10$	$-1.58 \pm 0.10$	1	k

<sup>a</sup>1: Zn; 2: Xray measurement; range includes assumed solar and  $\alpha$ -enhanced metal ratios in absorber with a solar O abundance of 8.74, and Galactic gas with ISM metallicity (see Turnshek et al. 2003); 3: Fe + 0.4; 4: Si, S, or O.

References. — a. Boissé et al. 1998; b. Turnshek et al. 2003; c. Churchill et al. 2000; d. RT00; e. de la Varga et al. 2000; f. Meyer et al. 1995; g. Rao, Turnshek, & Nestor 2004 [N(HI) measurements]; h. Khare et al. 2004 [N(ZnII) measurements]; i. Pettini et al. 2000; j. Turnshek et al. 2004; k. This work.

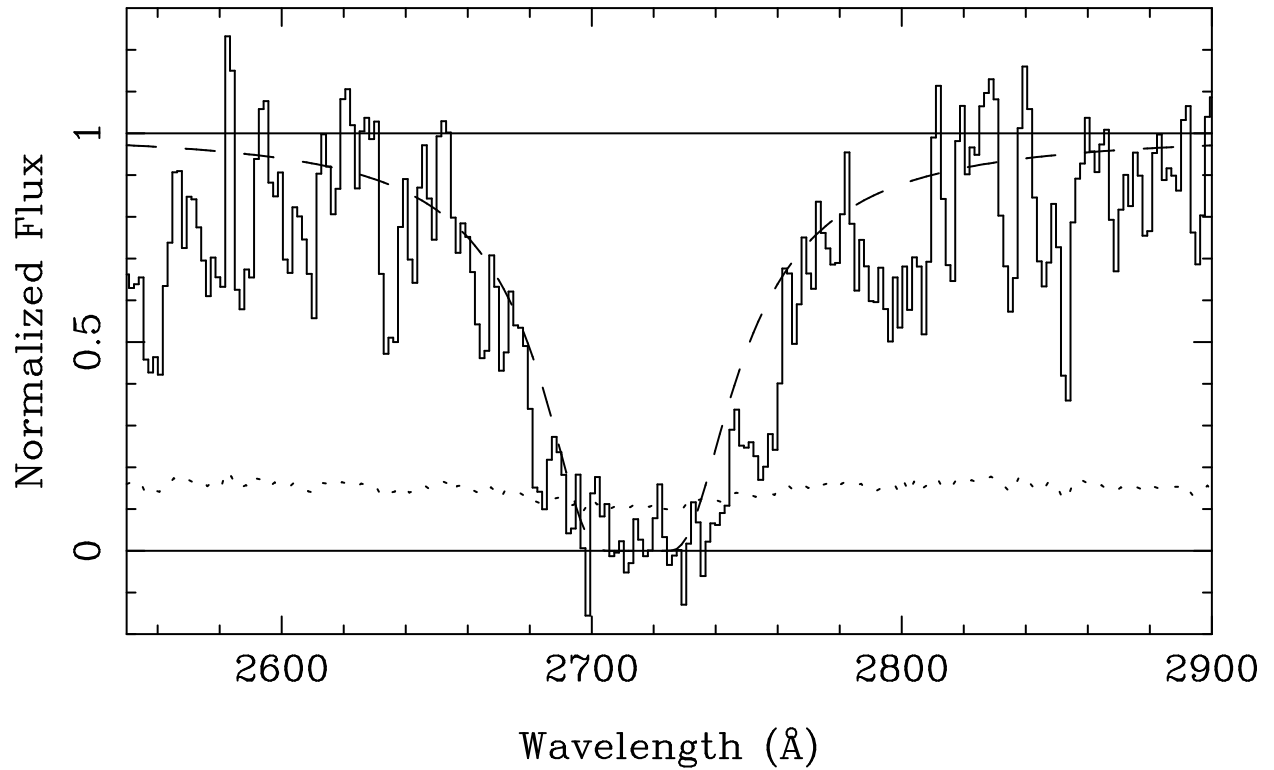


Fig. 1.— Part of the *HST*-STIS G230L spectrum of Q0948+433 showing the DLA line at  $2715\text{\AA}$  ( $z_{abs} = 1.233$ ). The dashed line is a Voigt profile convolved with the line spread function of the *HST*-STIS G230L grating and has column density  $N(HI) = 4.2 \times 10^{21} \text{ cm}^{-2}$ . The  $1\sigma$  error array is shown as a dotted line.

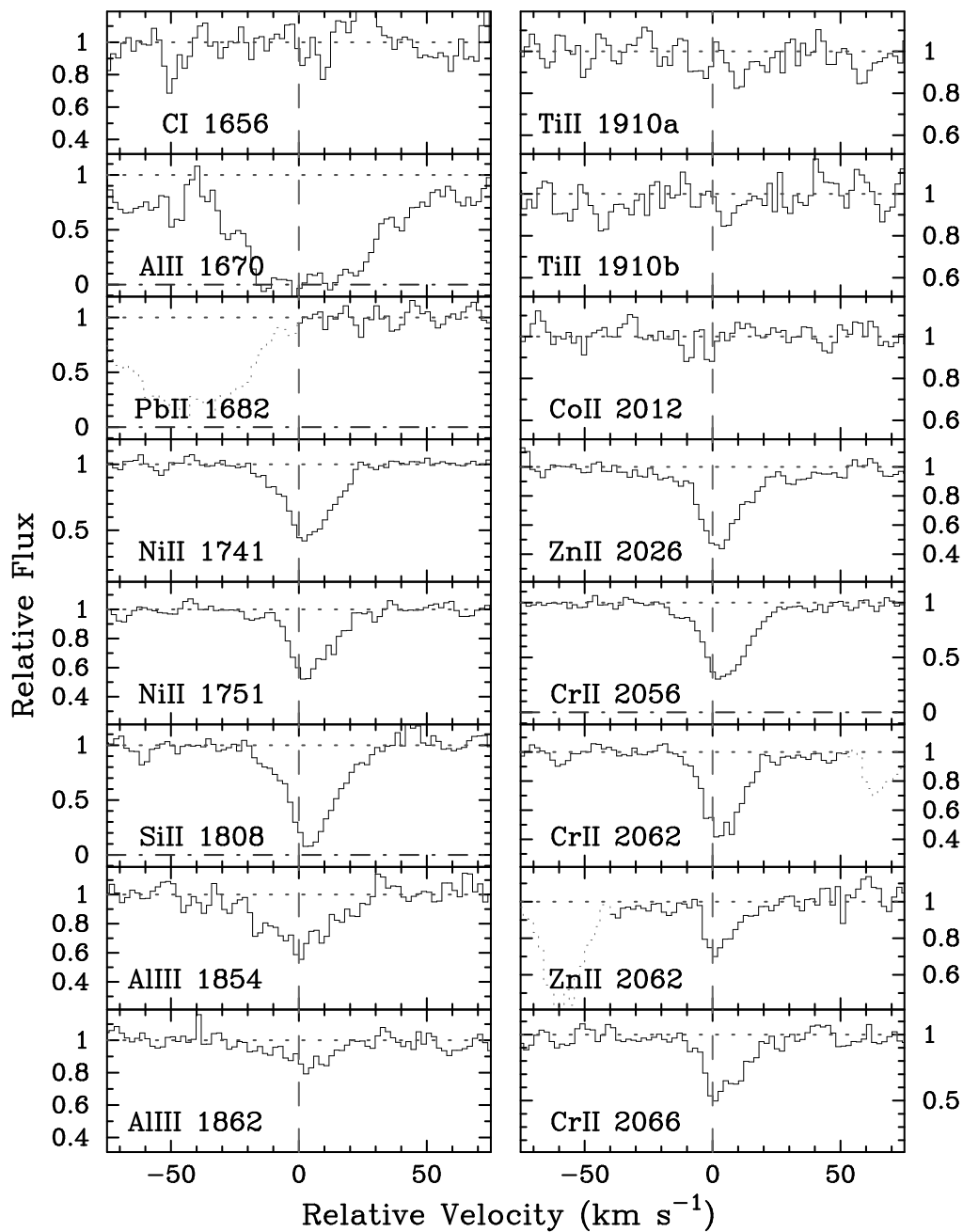
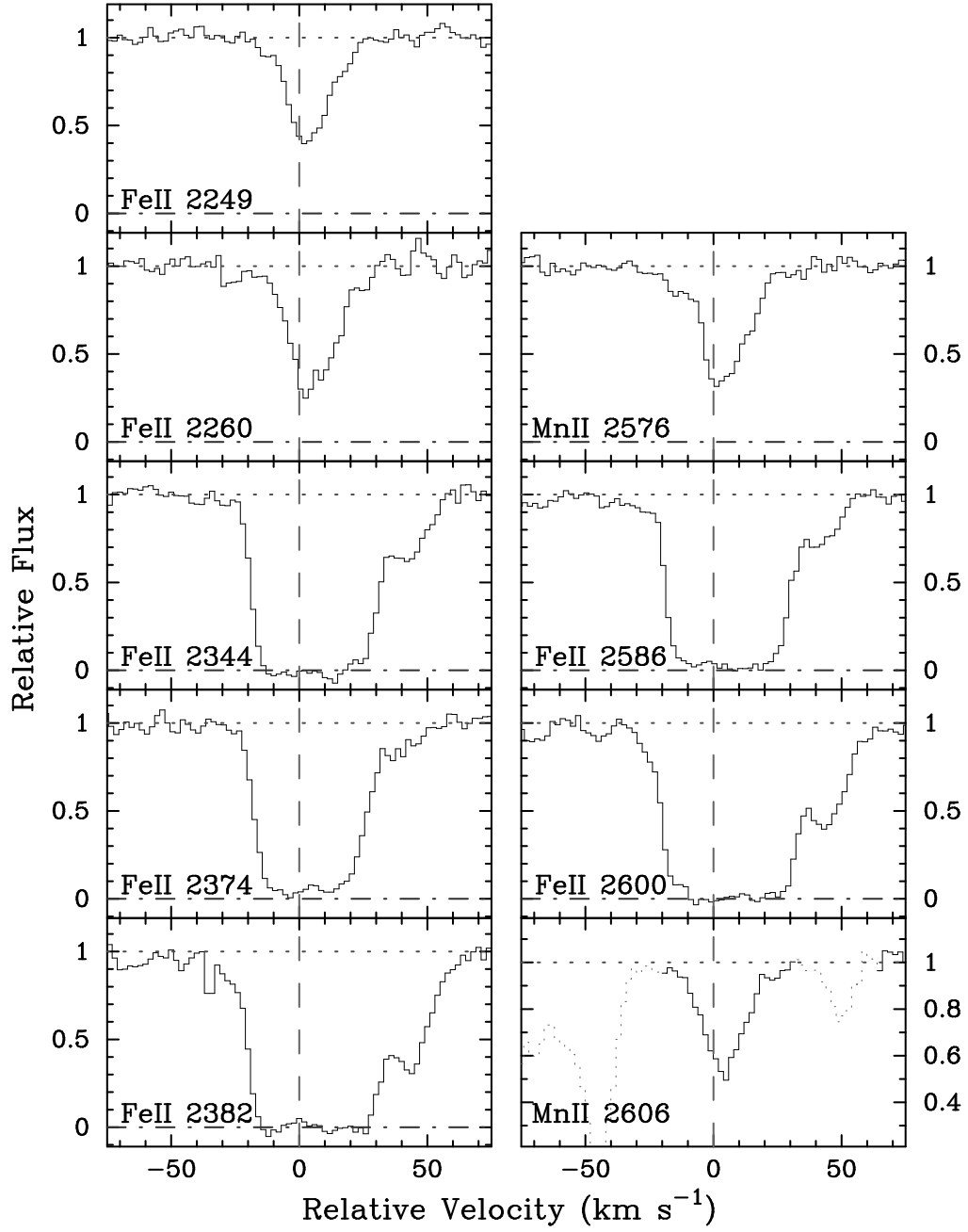


Fig. 2.— Velocity plot of the metal lines in the  $z = 1.479$  DLA toward Q0933+733. The velocity zeropoint was chosen arbitrarily to match the peak optical depth of the Cr II  $\lambda 2066$  profile.



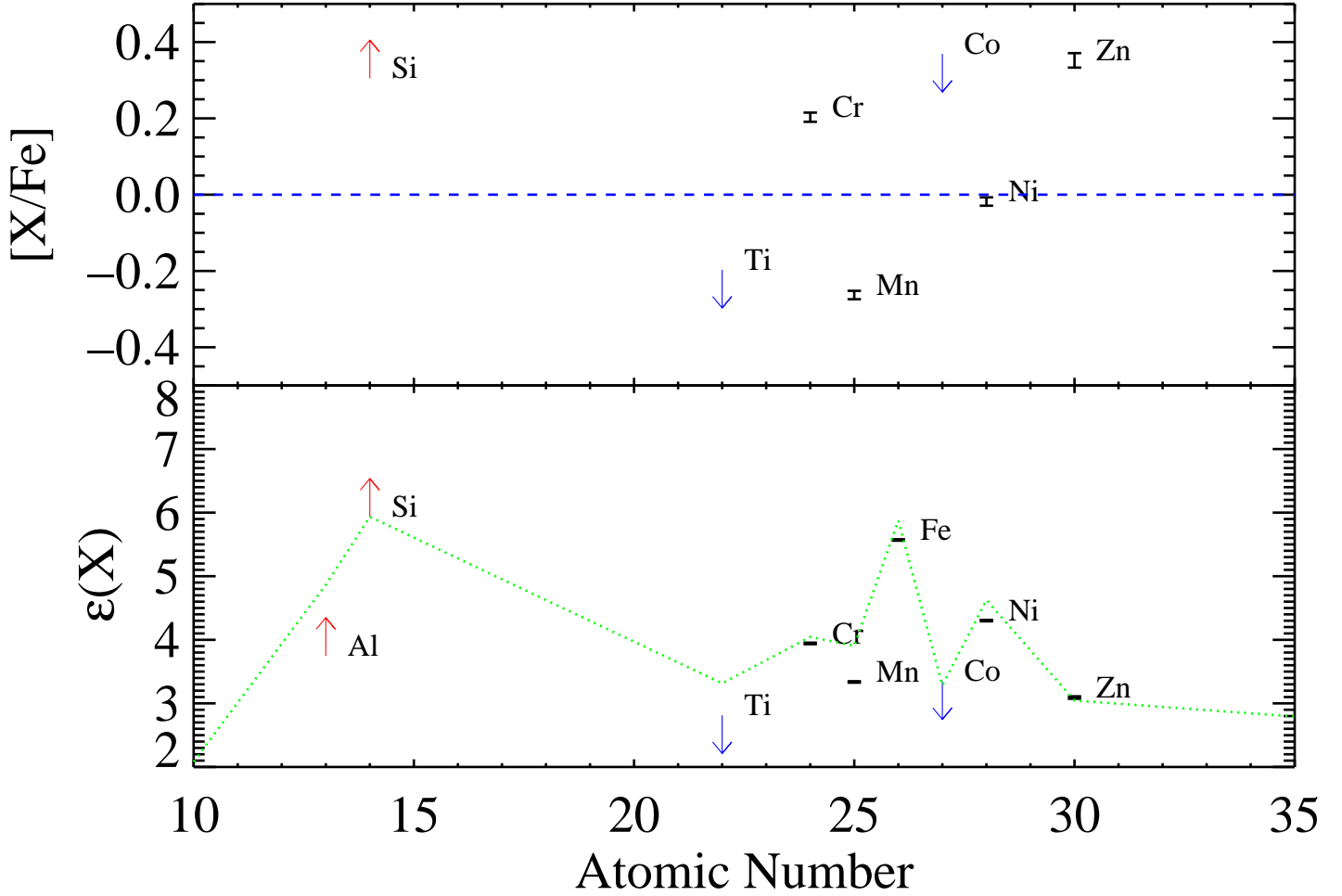


Fig. 3.— Relative abundances in the  $z = 1.479$  DLA toward Q0933+733. The top panel shows the abundances relative to Fe and the bottom panel gives the absolute abundances on a logarithmic scale with hydrogen at  $\varepsilon(H) = 12.0$ . The dotted line traces the solar abundance pattern scaled to match the Zn abundance in the  $z = 1.479$  DLA. These are gas phase abundances uncorrected for depletion.

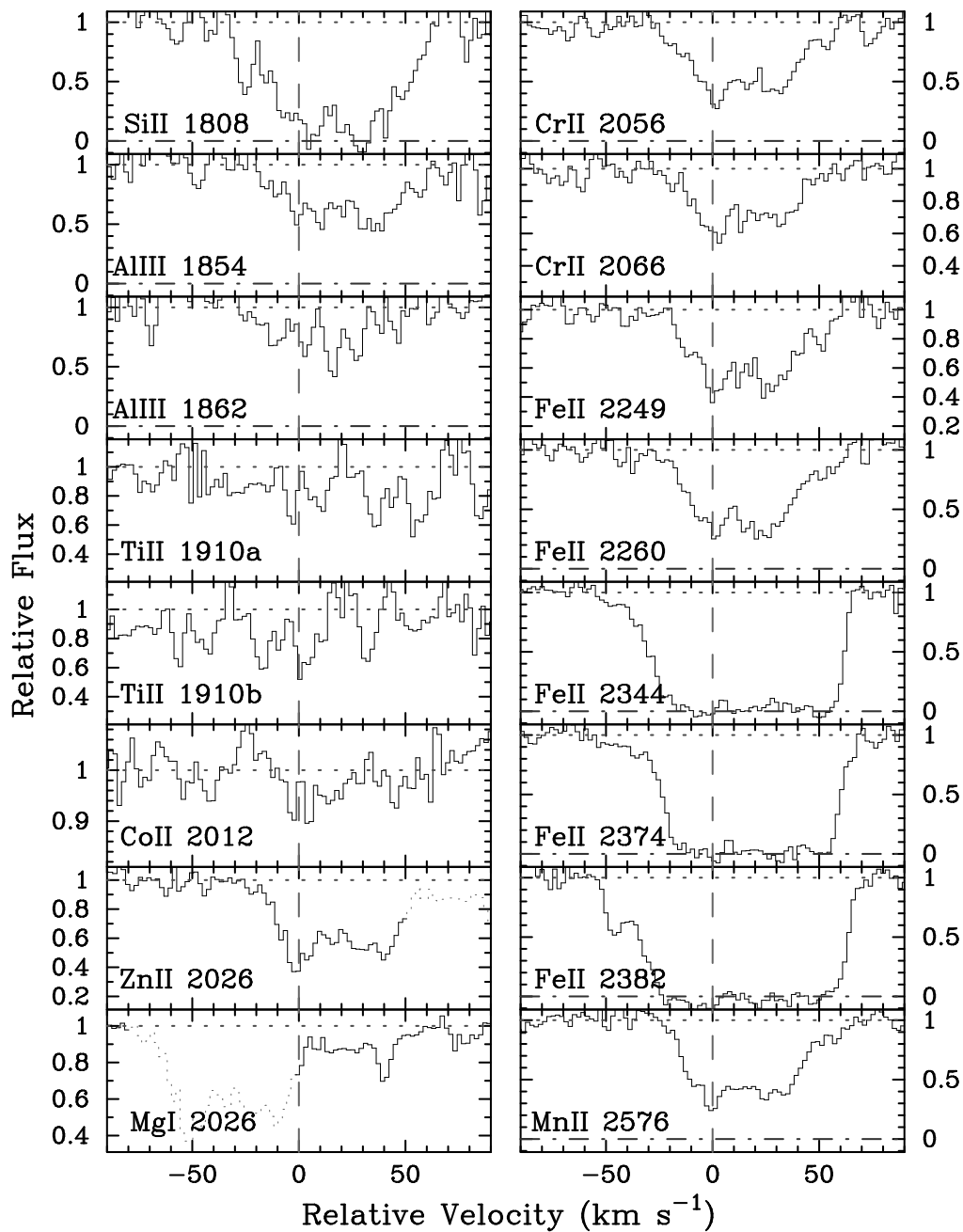
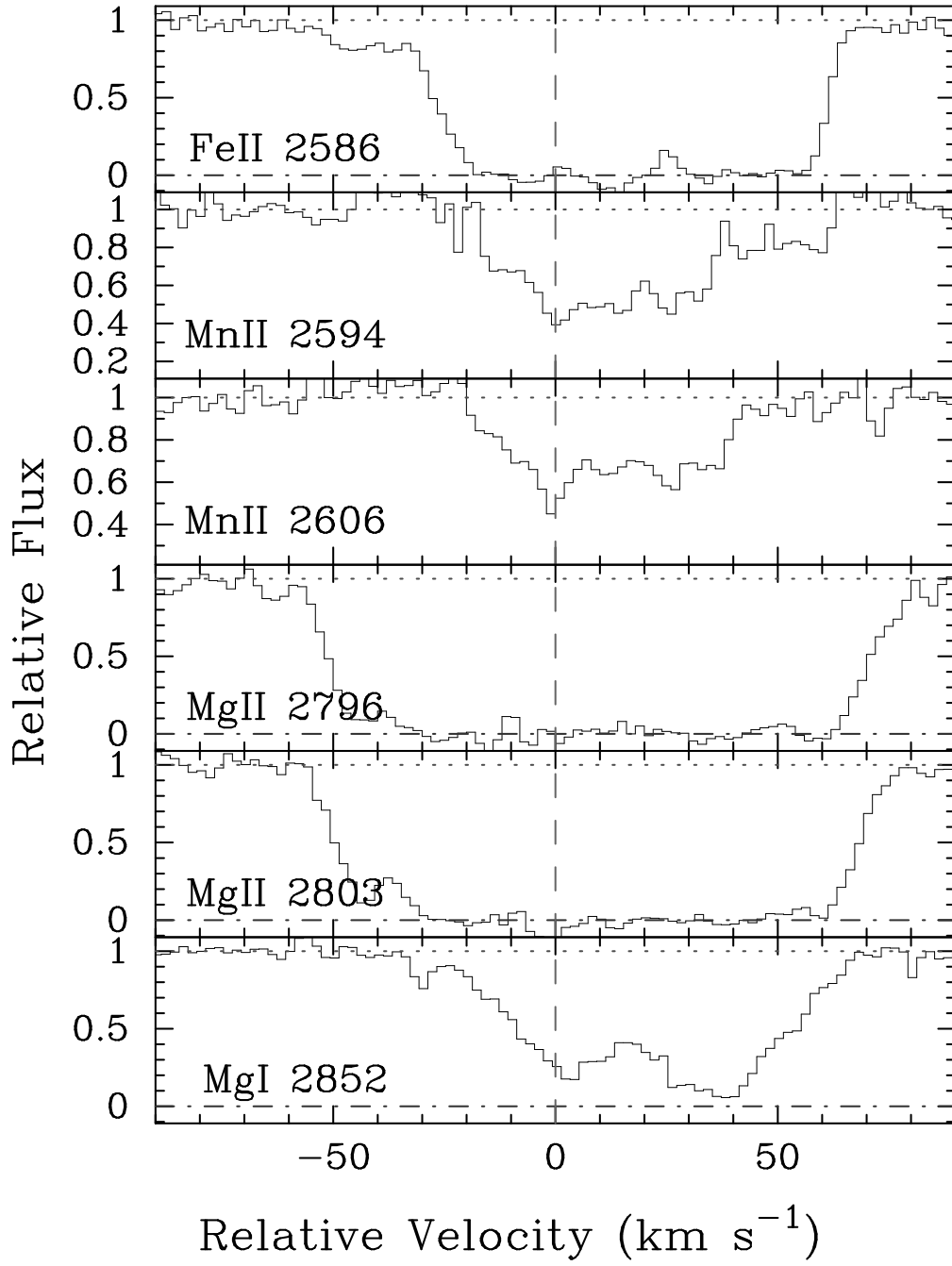


Fig. 4.— Velocity plot of the metal lines in the  $z = 1.233$  DLA toward Q0948+433. The velocity zeropoint was chosen arbitrarily to match the peak optical depth of the Mn II  $\lambda 2576$  profile.





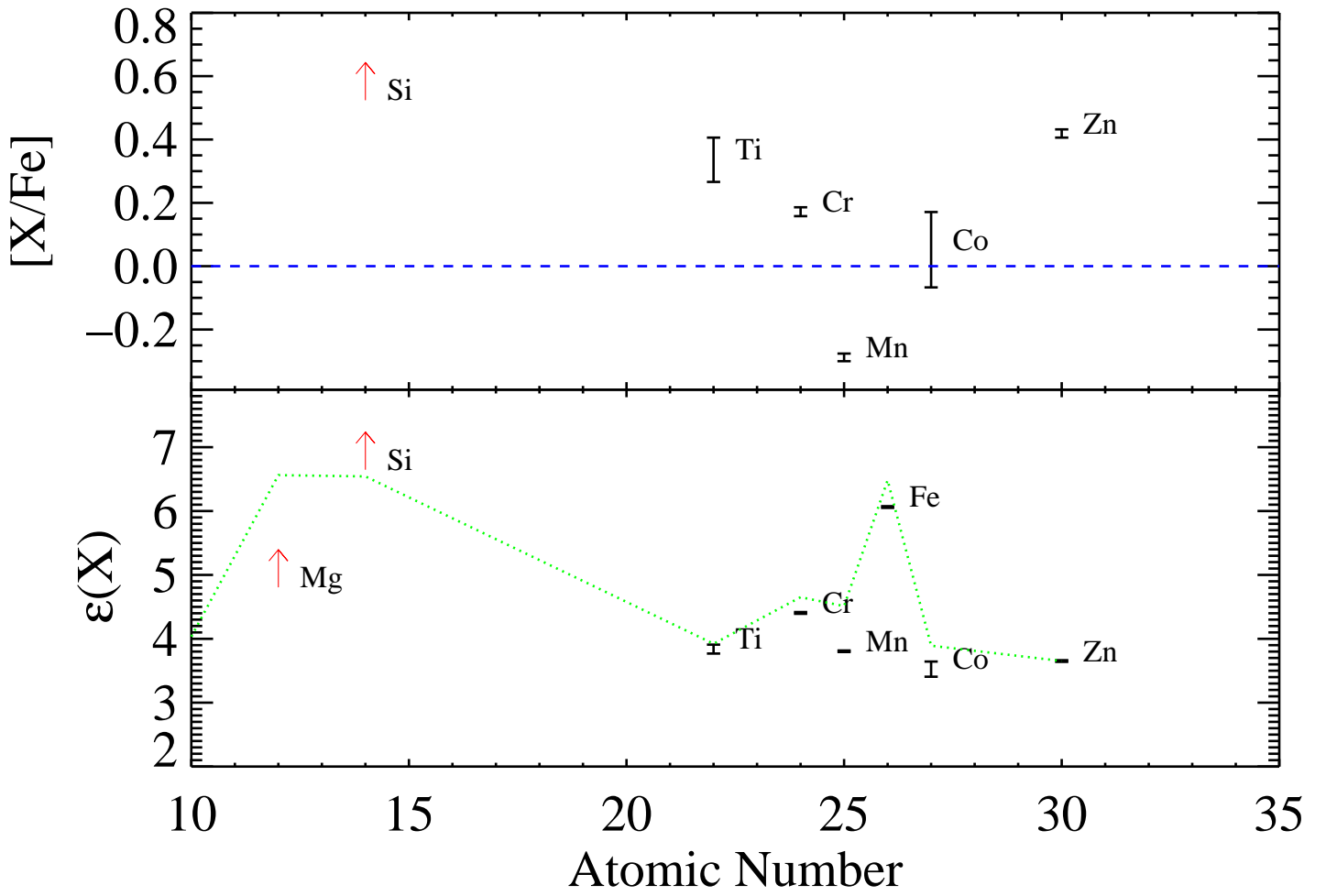


Fig. 5.— Same as for Figure 3, but for the  $z = 1.233$  DLA toward Q0948+433.

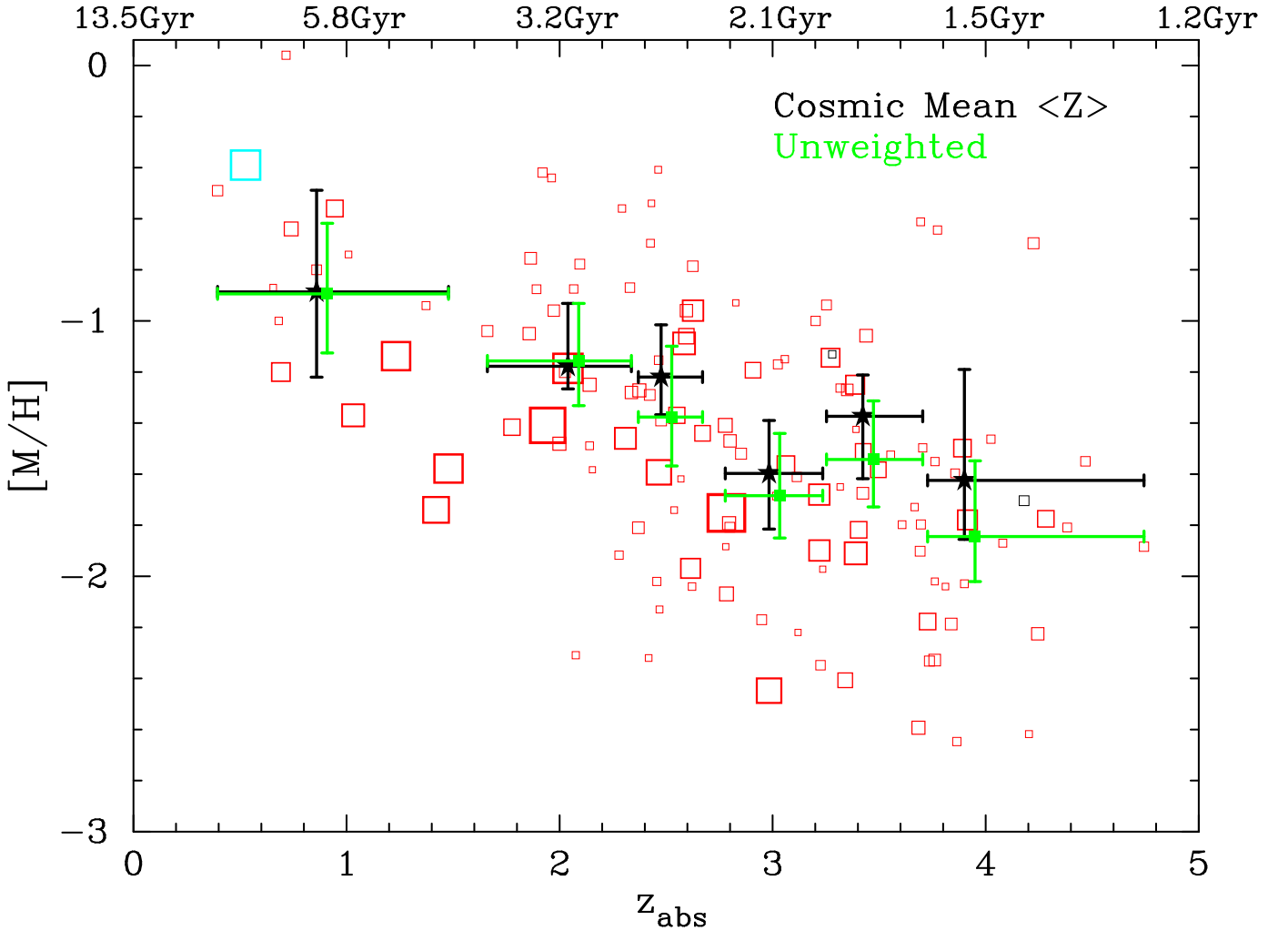


Fig. 6.— Metallicity  $[M/H]$  vs.  $z_{abs}$  for DLAs plotted as open squares where the area of each square is proportional to  $N(HI)$ . The X-ray measurement of  $[M/H]$  for the DLA toward Q0235+164 is plotted as the blue open square. All other measurements are derived from UV or optical quasar spectroscopy. DLAs with larger values of  $N(HI)$  dominate the  $N(HI)$ -weighted mean metallicity. This cosmic mean metallicity,  $\langle Z \rangle$ , is plotted for six bins and shown as black filled stars. Green filled squares are unweighted mean metallicities. Errors are 95% confidence limits determined using a bootstrap technique. The lowest redshift value of  $\langle Z \rangle$  is now more secure since the number of available  $[M/H]$  measurements has nearly doubled since the Prochaska et al. (2003b) analysis. The higher redshift points are adopted from Prochaska et al. (2003b). The best-fit slope to the  $\langle Z \rangle$  vs.  $z_{abs}$  data points, assuming a linear solution, is  $m = -0.26 \pm 0.06$ , confirming the trend of increasing metallicity with cosmic time.